NOTICE: This material may be protected by Copyright Law
(Title 17, U.S. Code)

SAE International

An Integrated Model of Rolling and Sliding in Rollover Crashes

2012-01-0605
Published
04/16/2012

James Funk, Jeffrey Wirth, Enrique Bonugli and Richard Watson
Biodynamic Research Corp

Alan Asay
Woolley Engineering Research

Copyright © 2012 SAE International

doi:10.4271/2012-01-0605

ABSTRACT

Rollover crashes are often difficult to reconstruct in detail because of their chaotic nature. Historically, vehicle speeds in rollover crashes have been calculated using a simple slide-to-stop formula with empirically derived drag factors. Roll rates are typically calculated in an average sense over the entire rollover or a segment of it in which vehicle roll angles are known at various positions. A unified model to describe the translational and rotational vehicle dynamics throughout the rollover sequence is lacking. We propose a pseudo-cylindrical model of a rolling vehicle in which the rotational and translational dynamics are coupled to each other based on the average frictional forces developed during ground contacts. We describe the model as pseudo-cylindrical because vertical motion is ignored but the ground reaction force is not constrained to act directly underneath the center of gravity of the vehicle. The tumbling phase of a rollover is modeled in three distinct phases: an initial brief airborne phase between roll initiation and the first ground contact, an early phase in which relative sliding between the perimeter of the vehicle and the ground causes the roll rate to increase, and a later phase in which the vehicle rolls without sliding and the roll rate decreases. In the early phase, the average vehicle deceleration is higher and is governed by sliding friction. In the later phase, the average vehicle deceleration is lower and is governed by geometric factors. Model predictions were fit to data from 12 well-documented rollover crashes in order to derive empirical values for the model parameters. In 11 out of the 12 rollovers studied, the model predictions matched the actual results with good accuracy. The results validate the underlying physical principles of the model and provide data that can be used to apply the model to real world rollovers. The proposed model provides a physical basis for understanding vehicle dynamics in rollovers and may be used in certain cases to improve the accuracy of a rollover reconstruction.

INTRODUCTION

Rollover crashes have been studied extensively from an accident reconstruction perspective. Rollovers are difficult to model with precision because they involve complex three-dimensional vehicle dynamics and multiple impacts, often to the same part of the vehicle, occurring over a long period of time. Due to their chaotic nature and sensitivity to small changes in initial conditions, the individual impacts that occur in rollover crash tests are generally not repeatable or predictable. Efforts have been made to model individual impacts in rollover crash tests using either impulse-momentum equations [13] or computational modeling packages [12, 14]. However, the usefulness of complicated models in reconstructing real world crashes is limited by their fidelity and by the amount of information typically available to the reconstructionist.

In practice, real world rollovers are usually reconstructed using simple models. Historically and up to the present, vehicle speed during the tumbling phase of a rollover crash has been calculated using a simple slide-to-stop formula [4-5, 8-9, 11]. Recently, investigators have suggested that the accuracy of rollover reconstruction can be improved using a variable deceleration rate approach [3, 15]. There is good empirical support for such an approach. Detailed video-based reconstructions of rollover tests have shown that the deceleration rate of a tumbling vehicle in a rollover is not constant, but is typically higher during the early portion of

the rollover and lower during the later portion of the rollover [1, 3, 6-7, 11, 15, 17-18].

Vehicle roll rate is also typically calculated using simple methods. The average roll rate over the entire rollover or a portion of it is calculated by dividing the number of rolls by time, where time is calculated based on an assumption of constant deceleration in translational velocity. It has been observed in multi-rollover crash tests that the roll rate typically rises monotonically, usually peaks sometime in the early part the rollover, then decreases monotonically at a slower rate than it rose [1-2, 3, 6-7, 11, 13, 15, 17]. It has further been noted that the time of peak roll rate often coincides with a knee in the translational velocity vs. time curve, corresponding to a decrease in the vehicle's translational deceleration rate [1, 3, 17].

In this paper, we propose a model for rollover crashes in which the rotational and translational dynamics of a rolling vehicle are coupled to each other based on the average frictional forces developed during ground contacts. Somewhat similar models were proposed by Chen and Guenther [4] and Rose and Beauchamp [15]. The Chen and Guenther [4] model utilized a constant deceleration approach to model the translational velocity of the vehicle. They theorized that in the early part of a rollover, the roll rate of the vehicle increases due to Coulomb friction as a result of the tangential velocity of the vehicle perimeter being lower than the vehicle's translational velocity. In the later part of the rollover, they theorized that the opposite phenomenon occurs: the roll rate decreases because the tangential velocity of the vehicle perimeter exceeds the translational velocity of the vehicle's center of gravity, and the relative sliding between the ground and vehicle results in frictional forces that slow the roll velocity of the vehicle until it reaches its point of rest. Rose and Beauchamp [15] presented several approaches to modeling a variable deceleration rate during rollovers. These approaches were something of a hybrid between modeling empirical data and applying impulse-momentum equations they had previously developed for modeling individual ground impacts in rollovers [13]. However, their methods did not explicitly link translational and rotational vehicle dynamics throughout the rollover sequence.

In our model, we theorize that friction due to relative sliding between the vehicle perimeter and the ground is the mechanism by which the roll rate increases early in the rollover, in agreement with Chen and Guenther [4] and Rose and Beauchamp [15]. We propose that once the tangential velocity of the vehicle's perimeter catches up to the translational velocity of the vehicle's center of gravity, relative sliding between the vehicle's perimeter and the ground ceases, consistent with the findings of Rose and Beauchamp [15]. During the later part of the rollover, we propose that the vehicle rolls without sliding and decelerates both translationally and rotationally at a rate governed by geometric factors. Our proposed model is bilinear and allows for a prediction of the overall translational and rotational vehicle dynamics in an average sense during both phases of the rollover sequence. The proposed model predicts a higher level of translational deceleration early in the rollover compared to later in the rollover, with the transition occurring at the time of peak roll rate. Thus, the proposed model provides a theoretical explanation for several phenomena that have been observed empirically in high speed rollover tests.

THEORY

The proposed model is two-dimensional and focuses on the translational motion of the vehicle's center of gravity and the rotation of the vehicle about its roll axis. All motion is assumed to occur in the plane perpendicular to the longitudinal axis of the vehicle. Pitch, yaw, longitudinal motion, vertical motion, and impacts to the vehicle are all neglected. In high speed rollovers, there is typically a brief airborne phase immediately after all four tires lift off the ground and cease leaving tire marks. Our proposed model begins at the first vehicle-to-ground contact after roll initiation. In the equations that follow, parameters with a 0 subscript indicate values at the time of roll initiation (end of tire marks). Roll initiation defines the zero point for both time and distance. Parameters with a 1 subscript indicate values at the time of the beginning of the sliding rollover phase (or constant values throughout the sliding phase), defined by the initial vehicle-to-ground contact. Parameters with a 2 subscript indicate values at the time of the beginning of the rolling phase (or constant values throughout the rolling phase). Final values at the end of the rollover are denoted by the f subscript. The initial conditions at the time of first ground contact (t_1) are given by:

$$v_1 = v_0 \tag{1a}$$

$$d_1 = v_0 t_1 \tag{1b}$$

$$\omega_1 = \omega_0 \tag{1c}$$

$$\theta_1 = \theta_0 + \omega_0 t_1 \tag{1d}$$

Vehicle-to-ground interaction is modeled using a free body diagram (Figure 1). The vehicle is modeled as a cylinder in one important respect: vertical motion is neglected. Therefore, throughout the rollover, the vertical ground reaction force is simply the weight of the vehicle. Also, the height of the vehicle's center of gravity is assumed to be constant throughout the rollover and equivalent to the radius

(r) of a cylinder having a circumference equal to twice the sum of the overall height (H) and width (W) of the vehicle:

$$r = \frac{H + W}{\pi} \tag{2}$$

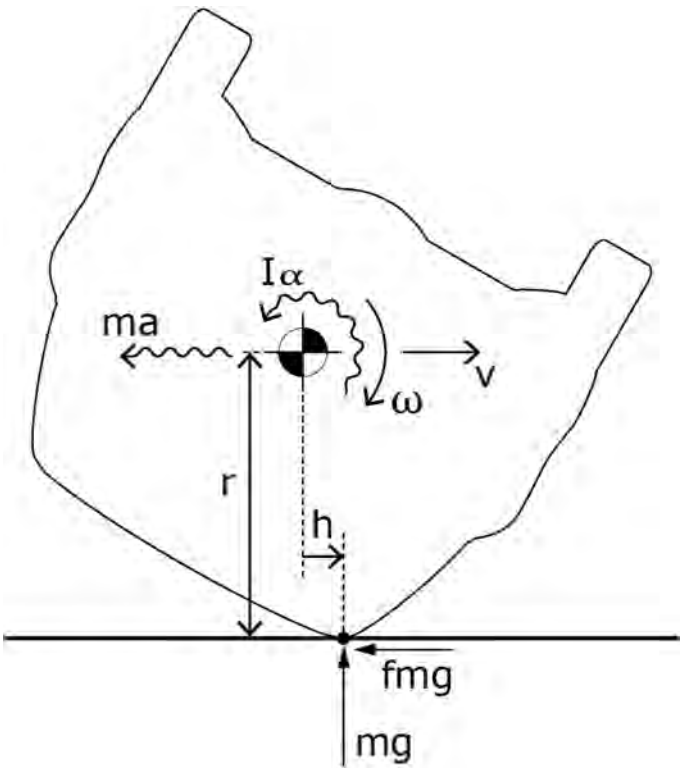

Figure 1. Free body diagram of a rolling vehicle.

A model of a purely cylindrical vehicle rolling on flat ground would place the contact point between the vehicle and ground directly below the vehicle's center of gravity. The problem with that approach is that the ground reaction force vector will always point behind the vehicle's center of gravity (if there is friction) or straight up through the vehicle's center of gravity (if there is no friction). In a purely cylindrical model, the ground reaction force vector can never act in front of the vehicle's center of gravity, and therefore the vehicle's roll rate can never decrease and the cylindrical vehicle can never stop rolling. The reason that a real vehicle slows down and eventually stops rolling is that it rolls more like a square wheel or a lumpy cylinder, with the impact point between the vehicle and the ground often being in front of the vehicle's center of gravity. In order to capture that necessary phenomenon in our model, we allowed the contact point between the perimeter of the vehicle and the ground (h) to be forward or rearward of the vehicle's center of gravity, with forward being defined as positive. Because relaxing the constraint that ground contact must occur directly below the vehicle's center of gravity implies a non-circular shape for the vehicle cross-section, we use the term "pseudo-cylindrical" to describe the model.

The interaction between the ground contact location and the magnitude of the frictional force acting on the vehicle determines whether the impact force vector passes behind the vehicle's center of gravity, causing the vehicle's roll rate to increase, or forward of the vehicle's center of gravity, causing the vehicle's roll rate to decrease. At the beginning of a rollover, there is usually relative sliding between the vehicle and the ground, because the tangential velocity of the perimeter of the vehicle is less than the translational velocity of the vehicle's center of gravity. Therefore, the highest possible frictional force is developed between the vehicle and the ground, which is the sliding coefficient of friction (f_s). Applying this kinetic constraint, the translational acceleration rate of the vehicle for the early "sliding" phase of the rollover (a_1) is obtained by summing the forces in the direction of travel and setting them equal to zero:

$$ma + fmg = 0 \tag{3}$$

Cancelling the vehicle mass (m) term and solving for (a) yields:

$$a_1 = -f_s g \tag{4}$$

The negative sign indicates that the vehicle is decelerating. Applying the constant deceleration rate from equation (4), the time-varying translational velocity and displacement of the vehicle during the sliding phase of the rollover ($t_1 < t < t_2$) is obtained from standard equations of motion:

$$v(t) = v_1 + a_1 g(t - t_1) \tag{5a}$$

$$d(t) = v_1(t - t_1) + \frac{1}{2} a_1 g (t - t_1)^2 \tag{5b}$$

The rotational acceleration rate (α) of the vehicle is obtained by summing the moments about the center of gravity of the vehicle and setting them equal to zero:

$$I\alpha + mgh - fmgr = 0 \tag{6}$$

where (I) is the roll moment of inertia of the vehicle about its center of gravity, which can also be expressed in terms of the vehicle's mass (m) and radius of gyration (k):

$$I = mk^2 \tag{7}$$

Substituting equation (7) into equation (6) and solving for (α) yields:

$$\alpha_1 = \frac{g}{k^2}\left(f_s r - h_1\right) \tag{8}$$

The time-varying roll velocity and roll angle of the vehicle during the sliding phase of the rollover ($t_1 < t < t_2$) are obtained from equations of motion:

$$\omega(t) = \omega_{init} + \alpha_1 t \tag{9a}$$

$$\theta(t) = \theta_{init} + \omega_{init} t + \frac{1}{2}\alpha_1 t^2 \tag{9b}$$

Unless the impact location (h_1) is far forward of the vehicle's center of gravity, the frictional force caused by the relative sliding between the perimeter of the vehicle and the ground will tend to increase the roll rate of the vehicle. As the roll rate of the vehicle increases and the translational speed of the vehicle decreases, the tangential velocity of the vehicle's perimeter catches up to the translational velocity of the vehicle's center of gravity. When those velocities equalize, the following kinematic constraint is satisfied:

$$v = \omega r \tag{10}$$

The time at which relative sliding between the vehicle and ground stops (t_2) is obtained by substituting equations (5a) and (9a) into equation (10) and solving for t:

$$t_2 = t_1 + \frac{v_1 - \omega_1 r}{\alpha_1 r + f_s g} \tag{11}$$

This time point marks the transition between the early phase of the rollover, in which the vehicle rolls and slides along the ground, and the later phase of the rollover, in which the vehicle rolls over the ground without sliding. For brevity, these phases will be termed the "sliding" and "rolling" phases, respectively. The translational velocity (v_2), distance from the trip point (d_2), roll velocity (ω_2), and roll angle (θ_2) at this transition point can be calculated by substituting equation (10) into equations (5a), (5b), (9a), and (9b), respectively.

Once there is no longer any relative sliding between the vehicle and the ground, the frictional force acting on the vehicle is no longer constrained to be the maximum available friction force. Instead, the frictional force will be whatever value satisfies the kinematic constraint in equation (10) and prevents relative sliding between the vehicle and the ground, so long as the frictional force required to do so does not exceed the maximum available friction force (f_s). The frictional force (f_2) acting during the rolling phase of the rollover is obtained by expanding equation (10) with substitutions of equations (5a), (9a), and (8) (substituting 2 for 1 in the subscripts):

$$v_2 - f_2 g\left(t - t_2\right) = \omega_2 r + \frac{gr}{k^2}\left(f_2 r - h_2\right)\left(t - t_2\right) \tag{12}$$

Since the kinematic constraint in equation (10) applies at the time of transition between the first and second phases of the rollover, it is known that $v_2 = \omega_2 r$. Once these terms are dropped out, the time variable ($t - t_2$) also cancels, yielding the following constant friction value for the rolling phase of the rollover:

$$f_2 = \frac{rh_2}{r^2 + k^2} \tag{13}$$

The acceleration rate (a_2) during the rolling phase of the rollover sequence is calculated by summing the forces along the direction of vehicle travel, setting them equal to zero (equation 2), and solving for (a):

$$a_2 = -\frac{rgh_2}{r^2 + k^2} \tag{14}$$

This value is constant and depends only on geometric factors. Applying the constant deceleration rate from equation (14), the time-varying translational velocity and displacement of the vehicle during the rolling phase of the rollover ($t_2 < t < t_f$) is obtained from standard equations of motion:

$$v(t) = v_2 + a_2 g\left(t - t_2\right) \tag{15a}$$

$$d(t) = d_2 + v_2\left(t - t_2\right) + \frac{1}{2}a_2\left(t - t_2\right)^2 \tag{15b}$$

The rotational acceleration rate (α_2) of the vehicle is obtained by summing the moments about the center of gravity of the

vehicle, setting them equal to zero (equation 6), substituting equations (7) and (13), then solving for (α):

$$\alpha_2 = -\frac{gh_2}{r^2 + k^2} \tag{16}$$

The time-varying roll velocity and roll angle of the vehicle during the rolling phase of the rollover ($t_2 < t < t_f$) are obtained from equations of motion:

$$\omega(t) = \omega_2 + \alpha_2 (t - t_2) \tag{17a}$$

$$\theta(t) = \theta_2 + \omega_2 (t - t_2) + \frac{1}{2}\alpha_2 (t - t_2)^2 \tag{17b}$$

The rollover ends when the translational and roll velocities reach zero. The total rollover time (t_f) is obtained by setting ω = 0 in equation (17a) and solving for (t):

$$t_f = t_2 + \frac{\omega_2}{\alpha_2} \tag{18}$$

The final roll distance (d_f) and roll angle (θ_f) are obtained by substituting equation (18) into equations (15b) and (17b), respectively.

The end result is a bilinear model of vehicle dynamics between the first ground contact and rest (Figure 2). The essential parameters of the model can be concisely summarized with only four parameters (Table 1). These four parameters are the constant translational and rotational acceleration rates for the sliding and rolling phases of the rollover. The predicted translational deceleration is higher in the first phase of the rollover than the second phase. The predicted roll velocity is a triangular-shaped function in which the peak roll rate occurs at the transition between the first and second phases of the rollover.

Table 1. Model parameters.

Rollover phase	Translational acceleration (a)	Roll acceleration (α)
Sliding ($t_1 < t < t_2$)	$-f_s g$	$\frac{g}{k^2}(f_s r - h_1)$
Rolling ($t_2 < t < t_f$)	$-\frac{rh_2 g}{r^2 + k^2}$	$\frac{-gh_2}{r^2 + k^2}$

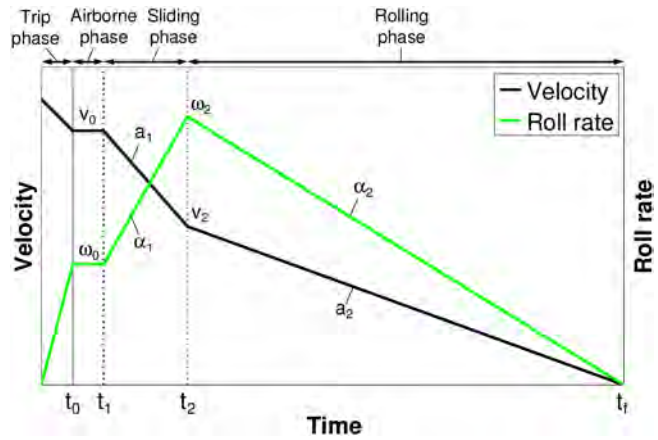

Figure 2. Illustration of vehicle dynamics predicted by the proposed rollover model.

Although a real vehicle rollover consists of a series of discrete ground impacts, the model proposed here neglects impacts and assumes constant deceleration in each phase of the rollover. This approach is commonly used in other areas of accident reconstruction. For example, skip skids and pedestrian tumbling also consist of a series of discrete ground impacts and airborne phases, but they are modeled using a constant deceleration assumption. This assumption is valid because the average deceleration of an object that tumbles to a stop in a series of ground impacts and airborne phases is equivalent to the constant deceleration that would occur due to simple frictional sliding [16]. Therefore, the proposed model should accurately predict the rollover dynamics in an average sense. However, some error in the calculated vehicle dynamics is expected at intermediate points in the rollover sequence, due to the chaotic nature of the individual ground impacts.

METHODS

The goal of this paper was to validate the theoretical model using data from rollover crashes in which the relevant vehicle dynamics throughout the rollover could be determined in detail. Specifically, it was necessary to determine the time histories for the vehicle's roll rate and the translational velocity of the vehicle's center of gravity. Although roll rate time histories have been published for a large number of rollover crash tests and real world rollover crashes, relatively few investigators have conducted the detailed video-based analysis necessary to obtain the translational velocity time history of a rolling vehicle. We were able to extract sufficiently accurate and detailed vehicle dynamics data from 11 rollover crash tests and 1 real world rollover described in the literature [1-2, 11, 17-18]. This sample includes 3 dolly rollover tests, 8 steer-induced rollover crash tests, and 1 steer-induced real world rollover (Table 2). All of the rollovers studied were high-speed, multi-roll events.

Table 2. Summary of rollovers analyzed.

Test ID	Vehicle	r (ft)	k (ft)	Reference	Test #	Test type	Surface	# Rolls
O5	1983 Chevrolet Malibu	3.34	2.08	Orlowski et al. [11]	5	Dolly	Pavement	3.5
O6	1983 Chevrolet Malibu	3.34	2.08	Orlowski et al. [11]	6	Dolly	Pavement	2
T6	1981 Dodge Challenger	3.10	2.01	Thomas et al. [18]	6	Dolly	Dirt	3
S0	1989 Ford Aerostar	3.85	2.23	Stevens et al. [17]	0	Steer	Pavement	2.5
S1	2001 Chevrolet Blazer	3.55	2.24	Stevens et al. [17]	1	Steer	Pavement/Dirt	9
S2	2002 Ford Explorer Sport	3.66	2.25	Stevens et al. [17]	2	Steer	Pavement/Dirt	5
S3	1997 Ford Explorer Sport	3.66	2.27	Stevens et al. [17]	3	Steer	Dirt	3.5
S4	1995 Nissan Pathfinder	3.53	2.26	Stevens et al. [17]	4	Steer	Dirt	3
A1	1996 Oldsmobile Bravada	3.47	2.30	Asay et al. [2]	1	Steer	Dirt/Pavement	10.5
A2	1991 Isuzu Rodeo	3.61	2.28	Asay et al. [2]	2	Steer	Dirt	7
A8	1991 Mitsubishi Montero	3.71	2.27	Asay et al. [2]	8	Steer	Dirt/Pavement	8.5
AN	2003 Ford Explorer Sport	3.66	2.25	Anderson et al. [1]	-	Real world	Pavement/Dirt	6

Data from two dolly rollover tests conducted by Orlowski et al. [11] and one dolly rollover conducted by Thomas et al. [18] were obtained by digitizing the graphs published in the papers. Data from a reconstructed real world rollover were published in tabular form by Anderson et al. [1]. Digital data from five steer-induced rollover tests were provided to us by Stevens et al. [17]. Data for three steer-induced rollover tests were obtained from direct collaboration with Asay et al. [2] with additional analysis performed by the authors. This additional analysis resulted in estimates for the roll initiation velocities in tests A1, A2, and A8 that were 5 - 12 mph lower than the values reported by Asay et al. [2]. This discrepancy is due to differences in the methods of analysis. In the Asay tests the GPS and non-contact speed data became unreliable during the tripping process. The prior published trip speeds [2] were extrapolations from the last reliable speed measurement prior to the end of trip (uncorrected for antenna rotation). The trip velocities reported in the present study were calculated by dividing the distance of travel by the time of travel of the center of gravity of the vehicle during the initial airborne phase between trip and the first ground contact. The present method resulted in lower estimated trip speeds, which suggests that more speed reduction took place during the trip phase than previously reported in [2]. However, based on a sensitivity analysis, we estimate that our trip speed calculations could be in error by up to 6.8% - 10%.

Parameters of the proposed model were optimized by fitting the model predictions to the data from each rollover crashes. Three model parameters were fit to the data: the sliding coefficient of friction between the vehicle and the ground (f_s), and the locations of the effective contact point between the perimeter of the vehicle and the ground during the first (h_1) and second (h_2) phases of the rollover. Inputs to the model included the effective radius (r) and radius of gyration (k) of the vehicle; the translational velocity (v_0), roll rate (ω_0), and roll angle (θ_0) at the time of roll initiation; and the time of first ground contact after roll initiation (t_1). If these parameters were not provided in the published data, we determined them through our own analysis. The three model parameters (f_s, h_1, and h_2) were optimized such that the predicted translational and rotational vehicle dynamics matched the known values as closely as possible. Predicted translational vehicle dynamics were fit to either a set of discrete vehicle positions at known times or a reconstructed velocity vs. time curve, depending on what data were available. Predicted rotational vehicle dynamics were fit to either a set of discrete roll angles at known times or a measured roll rate vs. time curve, depending again on what data were available. The model parameters were constrained to predict the exact roll distance (d_f) and number of rolls (θ_f) that occurred in the actual rollover. The goodness of fit of the models was quantified using the correlation coefficient (R^2). The optimization was accomplished by using the Solver routine in Microsoft Excel to maximize the average R^2 value of both the translational and rotational vehicle dynamics. Different variations on this optimization scheme were investigated and found to have a minimal effect on the results.

RESULTS

The overall vehicle dynamics in the rollover crashes studied were remarkably similar. In accordance with the predictions of the model, the translational over-the-ground velocity of the rolling vehicles typically decelerated more quickly in the early part of the rollover and more slowly later in the rollover. Likewise, the roll rate typically increased rapidly just before four wheel lift, leveled briefly during the vehicle's initial airborne phase, increased again as the vehicle slid while rolling, then decreased during the later part of the rollover as the vehicle rolled without sliding. In all tests, the calculated relative sliding velocity between the perimeter of the vehicle and the ground ($v - \omega r$) was highest at the initiation of the rollover, then decreased to approximately zero and remained there until the end of the rollover (Figure 3). There were no instances where the tangential velocity of

the vehicle perimeter exceeded the translational velocity of the center of gravity of the vehicle to an extent that exceeded the calculation error. Models fit with optimized parameters replicated the vehicle dynamics with good accuracy in 11 out of the 12 rollover crashes studied (Figures App1, App2, App3, App4, App5, App6, App7, App8, App9, App10, App11, App12 in the Appendix). The models fit the rotational vehicle dynamics well ($R^2 > 0.76$ in all tests) and the translational vehicle dynamics exceptionally well ($R^2 > 0.95$ in all tests) (Table 3).

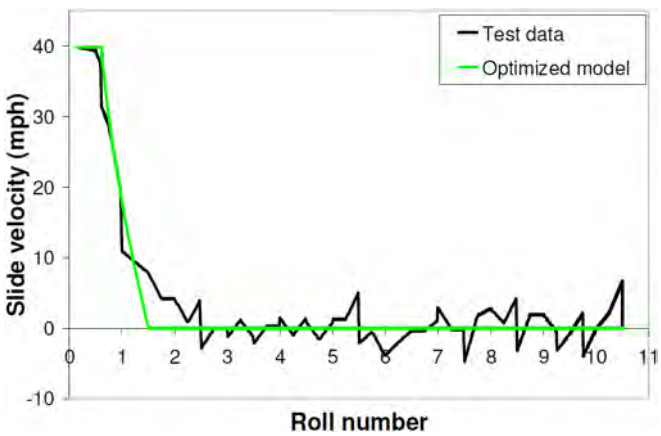

Figure 3. Relative sliding velocity between the perimeter of the vehicle and the ground (v-ωr) for test A1.

The only rollover crash that the model could not fit well was test S0. In this test, the vehicle's roll rate decreased upon landing after the initial airborne phase, rather than increasing like all the others (Figure App6). This unexpected behavior occurred because the vehicle landed on its far side roof rail just after the one half roll point and slid for some distance. After nearly stopping its rotation, the vehicle suddenly began rolling again while still sliding. Thereafter, the vehicle dynamics were typical of the other rollover crashes. The sliding phase of this crash could not be effectively modeled in an average sense because the rollover dynamics varied so dramatically. Therefore, it was necessary to break the sliding phase of the rollover into two parts when modeling test S0. The sliding coefficient of friction f_s was assumed to remain constant throughout both parts of the sliding phase, but the location of ground contact (h_1) was assumed to differ in the two parts of the sliding phase. The effective impact location (h_1) was quite far forward of the vehicle's center of gravity (2.80 feet) as the roll rate initially slowed down, but moved to point closer to the vehicle's center of gravity (0.68 feet) when the vehicle began rolling again (Table 3). Using this modified approach, the model was able to effectively model the vehicle dynamics of test S0.

There was considerable variation in the values of the optimized model parameters. Nonetheless, certain trends emerged. The optimized coefficient of friction (f_s) values varied widely (0.48 - 1.48), reflecting deceleration kinematics that ranged from sliding over a hard surface to digging into a soft surface. The average contact locations between the vehicle perimeter and the ground were always in front of the vehicle's center of gravity, typically by about a foot and a half. The method by which the rollover was initiated (dolly vs. steer) did not appear to have much effect on the vehicle dynamics. However, the type of surface over which the vehicle traveled when it was in the sliding phase of the rollover appeared to strongly affect the vehicle dynamics during the sliding phase of the rollover. It was observed that the translational and roll acceleration rates during the sliding phase of the rollover were correlated, with higher values seen in vehicles that slid over dirt compared to pavement (Figure 4). During the rolling phase of the rollover, the translational and roll deceleration rates were even more highly correlated, as expected (Figure 5). However, the surface over which the vehicle rolled did not appear to affect its deceleration rate during this stage of the rollover. The deceleration rates during the rolling portion of the rollover ranged from 0.21 - 0.40. These values were considerably lower than the sliding friction coefficients, which would be expected since the vehicles were generally not sliding during this phase of the rollover.

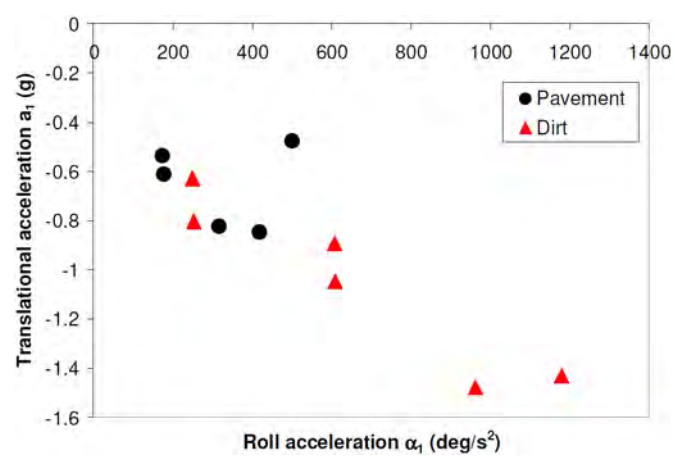

Figure 4. Relationship between fit values for translational and roll acceleration during the sliding phase of the rollovers (excluding test S0).

Table 3. Results of the model fits.

Test ID	O5	O6	T6	S0*	S1	S2	S3	S4	A1	A2	A8	AN	Ave ± SD
Optimized parameters													
f_s	0.48	0.85	0.89	0.54	0.82	0.61	0.63	0.80	1.43	1.05	1.48	0.54	0.84 ± 0.33
h_1 (ft)	0.42	1.85	1.45	2.80, 0.68	2.07	1.75	1.60	2.14	1.60	2.07	2.80	1.49	1.75 ± 0.59
h_2 (ft)	1.46	1.61	0.95	1.07	1.09	1.34	1.35	2.00	1.30	1.45	1.38	1.18	1.35 ± 0.28
h_1/r	0.13	0.55	0.47	0.73, 0.18	0.58	0.48	0.44	0.61	0.46	0.57	0.75	0.41	0.50 ± 0.16
h_2/r	0.44	0.48	0.31	0.28	0.31	0.37	0.37	0.57	0.37	0.40	0.37	0.32	0.38 ± 0.08
R^2 (trans)	0.97	0.95	0.98	1.00	1.00	1.00	1.00	1.00	1.00	1.00	1.00	1.00	0.99 ± 0.01
R^2 (rot)	0.82	0.76	0.78	0.92	0.94	0.94	0.97	1.00	0.99	0.96	0.99	0.99	0.92 ± 0.08
Other parameters													
a_1 (g)	-0.48	-0.85	-0.89	-0.54	-0.82	-0.61	-0.63	-0.80	-1.43	-1.05	-1.48	-0.54	-0.84 ± 0.33
a_2 (g)	-0.31	-0.35	-0.22	-0.21	-0.22	-0.27	-0.27	-0.40	-0.26	-0.29	-0.27	-0.23	-0.27 ± 0.06
$a_{overall}$ (g)	-0.37	-0.53	-0.40	-0.36	-0.42	-0.38	-0.33	-0.57	-0.38	-0.38	-0.41	-0.39	-0.41 ± 0.07
α_1 (deg/s^2)	500	417	607	-273, 512	316	177	249	252	1179	609	962	173	495 ± 328
α_2 (deg/s^2)	-173	-192	-129	-100	-114	-134	-134	-210	-138	-147	-134	-117	-143 ± 33
t_1 (s)	0.06	0.19	0.07	0.22	0.26	0.25	0.25	0.22	0.44	0.42	0.43	0.28	0.26 ± 0.12
t_2 (s)	0.99	1.01	0.65	1.78	1.75	1.53	0.89	1.47	0.94	0.99	0.96	2.85	1.32 ± 0.61
t_f (s)	4.16	3.20	4.30	5.16	8.20	5.60	4.54	3.77	7.79	6.16	7.13	7.48	5.62 ± 1.70
ω_0 (deg/s)	85	75	115	231	263	319	332	171	360	407	325	100	232 ± 119
ω_2 (deg/s)	549	419	469	338	733	545	491	485	945	757	829	544	592 ± 182
θ_0 (rolls)	0.25	0.13	0.13	0.19	0.19	0.16	0.15	0.21	0.17	0.16	0.17	0.13	0.17 ± 0.04
θ_1 (rolls)	0.26	0.16	0.15	0.33	0.38	0.38	0.38	0.31	0.61	0.63	0.56	0.20	0.36 ± 0.16
θ_2 (rolls)	1.08	0.73	0.62	0.91	2.43	1.92	1.11	1.45	1.51	1.56	1.40	2.50	1.44 ± 0.61
θ_f (rolls)	3.5	2	3	2.5	9	5	3.6	3	10.5	7	8.5	6	5.3 ± 2.9
v_0 (mph)	32	32	29	34	58	41	30	42	55	46	54	54	42 ± 11
v_2 (mph)	22	17	17	15	31	24	21	20	39	33	37	24	25 ± 8
d_1 (ft)	3	9	3	11	22	15	11	14	35	28	34	22	17 ± 11
d_2 (ft)	39	38	23	67	119	76	35	71	69	61	69	169	70 ± 40
d_f (ft)	90	65	69	106	265	147	93	105	266	184	234	249	156 ± 79
t_2/t_f	0.24	0.32	0.15	0.34	0.21	0.27	0.20	0.39	0.12	0.16	0.13	0.38	0.24 ± 0.10
θ_2/θ_f	0.31	0.37	0.21	0.36	0.27	0.38	0.31	0.48	0.14	0.22	0.16	0.42	0.30 ± 0.10
d_2/d_f	0.44	0.59	0.33	0.64	0.45	0.52	0.38	0.67	0.26	0.33	0.29	0.68	0.46 ± 0.15

**Test S0 required the sliding phase to be broken into two parts with a single f_s value and two different h_1 values, both of which are given.*

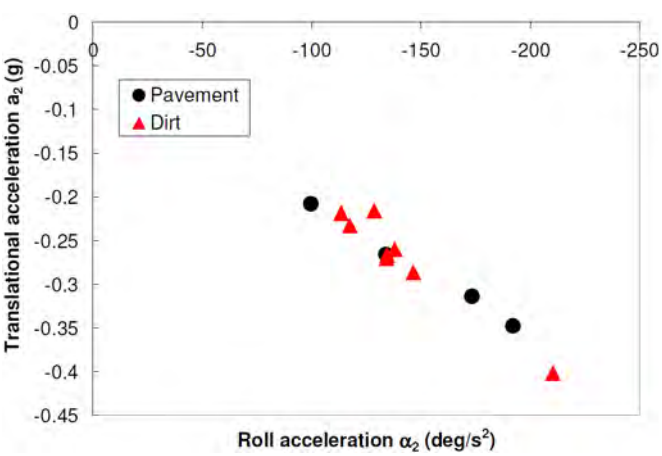

Figure 5. Relationship between fit values for translational and roll acceleration during the rolling phase of the rollovers.

Vehicles that slid on a dirt surface also stopped sliding relatively sooner than vehicles that slid on pavement. The transition from rolling and sliding to rolling without sliding can be quantified in terms of time, roll angle, or distance. This transition point corresponds to the time of peak roll rate and the knee in the translational velocity curve. On average, vehicles that rolled over dirt transitioned from sliding to rolling 19% of the way through the rollover in terms of time (t_2/t_f), 25% of the way through the rollover in terms of roll angle (θ_2/θ_f), and 38% of the way through the rollover in terms of distance (d_2/d_f). The corresponding numbers for vehicles that slid over pavement were 29%, 35%, and 55% for time, roll angle, and distance, respectively. Almost all of the vehicles that slid over dirt transitioned from sliding to rolling sooner than vehicles that slid over pavement. The one exception was test S4 in which the vehicle slid over dirt but transitioned from sliding to rolling relatively late in the rollover. However, it should be noted that the available data in terms of both translational and rotational vehicle dynamics

were rather sparse in this test (Figure App10). In general, model parameters affected by sliding dynamics (e.g., f_1 and d_2/d_f) were significantly affected by the type of ground surface, whereas model parameters that were governed by geometric factors (e.g. f_2 and h) were not (Figure 6).

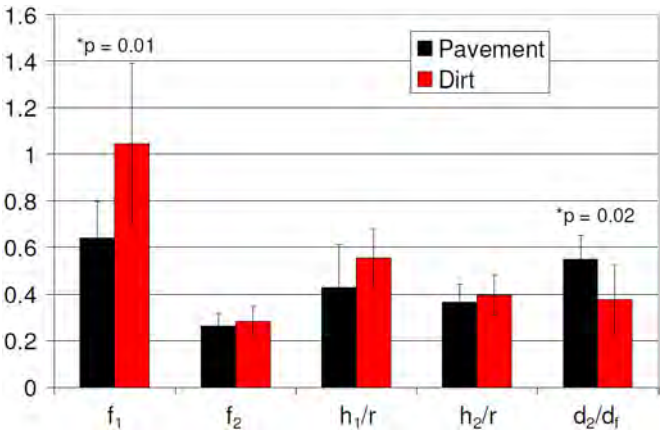

Figure 6. Comparison of optimized model parameters between rollovers occurring on pavement vs. dirt.

DISCUSSION

This paper presents a relatively simple analytical model based on the hypothesis that the tumbling phase of a rollover consists of three distinct phases: an initial brief airborne phase between roll initiation and the first ground contact, an early phase in which the vehicle rolls while also sliding along the ground, and a later phase in which the vehicle rolls without sliding. Model parameters that determine the translational and rotational acceleration rates of the vehicle during both the sliding and rolling phases of the rollover were fit to information from detailed reconstructions of 12 rollover crashes (Table 3). These results provide a starting point for the reconstructionist wishing to use this model. The accuracy of these optimized parameters was limited by the available data. In every case, there was substantially more and better information available pertaining to the rotational dynamics compared to the translational dynamics. In several rollover tests, a roll rate sensor provided excellent information. When integrated over time, the data from the roll rate sensors always predicted the total number of rolls with good accuracy. In cases where the vehicle was not instrumented with a roll rate sensor, video analysis was performed to obtain roll angles (usually in quarter roll intervals) at discrete time points. Although not as detailed as data from a roll rate sensor, the video analyses of the rotational vehicle dynamics provided good information. In several cases, video analysis results were validated by a favorable comparison to roll rate sensor measurements (analysis not shown).

On the other hand, translational vehicle dynamics were much more difficult to determine. Currently, there is no sensor that can be used to directly measure the translational velocity of a rolling vehicle. Painstaking analysis of video, ground, vehicle, and sensor evidence is required to accurately determine the location of the rolling vehicle's center of gravity at discrete time points. In some cases, the exact timing and location of the vehicle could only be determined with good accuracy at 3 or 4 positions between roll initiation and rest. As a consequence, it is difficult to accurately determine the translational deceleration of a rolling vehicle, particularly in lower severity rollovers where fewer intermediate vehicle positions can be pinpointed. Because the sliding coefficient of friction (f_s) was largely fit to the translational velocity data early in the rollover, this model parameter probably has the greatest uncertainty associated with its optimized values, which were quite variable. Optimized values for the effective ground contact locations (h_1 and h_2) utilized the roll rate data, as well, and are therefore probably more accurate.

In spite of the inevitable uncertainties, the analysis yielded intuitive results. The optimized sliding coefficient of friction (f_s) values ranged from 0.48 - 0.85 for vehicles rolling while sliding on pavement. Although these values are somewhat higher than the expected friction value for metal sliding on pavement, they are expected to be somewhat inflated because they incorporate the initial ground impact. For vehicles rolling while sliding on dirt, the optimized coefficient of friction (f_s) values were significantly higher, ranging from 0.63 - 1.48 ($p = 0.01$). This result was also expected, because a vehicle may encounter more mechanical resistance when digging into soft ground. The type of surface over which the vehicle rolled during the early portion of the rollover was the only factor that seemed to have a substantial effect on the results. We believe that the overall higher drag factors that have been reported for vehicles rolling over dirt as opposed to pavement [3, 10] are the result of increased friction during the early part of the rollover when the perimeter of the vehicle digs into the ground as it slides. Once the vehicle transitioned to rolling without sliding, we observed that its deceleration rate was governed by geometric factors, rather than the surface over which it was rolling. It is notable that our analysis confirmed that the average location of the ground force vector (h) was always in front of the vehicle's center of gravity during both phases of all the rollovers studied. This result was also expected given the non-cylindrical cross-sectional shape of a rolling vehicle. The effective ground contact location during the rolling phase (h_2) showed the least amount of variation, likely because the idiosyncratic effects of high-severity ground impacts were lower in the lower-energy later portion of the rollover. The average vehicle deceleration late in the rollover ranged from 0.21 - 0.40 in the 12 rollovers studied, which is in agreement with the analyses of previous investigators [1, 3, 17].

The main contribution of our model is that it provides a theoretical basis for linking the translational and rotational dynamics of a rolling vehicle throughout the rollover sequence based on the simple concept of Coulomb friction. The fact that we were able to achieve excellent fits with the empirical data from actual rollover crashes validates the theory behind the model. We believe that our model strikes a good balance between accuracy and complexity. As a bilinear model, it is more complex and accurate than a simple linear constant deceleration model (which is also implicitly based on the concept of Coulomb friction). However, it is much simpler than an impact-by-impact level reconstruction. Rose et al. [13, 15] presented a detailed impulse-momentum analysis that can be applied to individual ground impacts. Their equations are considerably more complex than ours because they incorporate vertical motion, but both approaches utilize the same physical principles. Although greater accuracy can be achieved by characterizing individual impacts, there is typically not enough information available in real world reconstructions to completely characterize each individual ground impact. Therefore, applying a physics-based model that is accurate in an average sense can be useful and practical.

Based on our sample of 12 rollover crashes, we conclude that the vehicle dynamics in a "typical" rollover will follow the general pattern shown in Figure 2. Rose and Beauchamp [15] have noted that roll rate time history often plateaus for a period of time near its peak, rather than following the predicted triangular pattern of Figure 2. We noticed that behavior in several of the rollovers we studied, as well. The physical interpretation of a plateau rather than a triangular peak in the roll rate data is that the vehicle transitioned from sliding to rolling upon landing from an airborne phase. Although our model does not distinguish ground impacts and airborne phases, the error associated with this simplifying assumption appeared to be minimal. However, the model predictions showed substantial error when the vehicle roll was "atypical" and did not follow the general pattern of vehicle dynamics shown in Figure 2. Test S0 is a good example of how successive individual impacts can have such different effects on the vehicle dynamics that it is simply not possible to lump them together and characterize them in an average sense. In test S0, the vehicle's roll rate decreased early in the roll and the vehicle slid for a long distance before the roll rate increased again. Wilson et al. [19] also conducted a steer-induced rollover test and reported unusual vehicle dynamics with a long period of sliding in the middle of the rollover. Both of these tests were conducted on pavement. These tests highlight the need for the reconstructionist to be alert for evidence that indicates a long period of sliding in the middle of a rollover or any other unusual vehicle dynamics.

CONCLUSIONS

1. Translational and rotational vehicle dynamics in a rollover crash are linked to each other based on the forces developed during ground contacts. A relatively simple model was developed in which the tumbling phase of a vehicle rollover was broken into three phases: an initial brief airborne phase between roll initiation and the first ground contact, an early phase in which sliding between the vehicle and the ground causes the roll rate to increase, and a later phase in which the vehicle rolls without sliding and the roll rate decreases. Using optimized frictional and geometric parameters, the model was able to match the vehicle dynamics of 12 rollover crashes in which detailed reconstruction information was available.

2. The model predicts that a rolling vehicle will decelerate in a bilinear fashion. In the rollovers studied, the deceleration rate was higher early in the rollover when the vehicle was rolling and sliding (0.84 ± 0.33 g) and lower in the later part of the rollover when the vehicle was rolling without sliding (0.27 ± 0.06 g). The roll acceleration values were 495 ± 328 deg/s^2 during the sliding phase and -143 ± 33 deg/s^2 during the rolling phase of the rollover. The average deceleration from the end of tire marks to rest was 0.41 ± 0.07 g.

3. The deceleration rate during the sliding phase of the rollover was significantly higher when the vehicle was rolling and sliding on dirt (1.05 ± 0.34 g) as opposed to pavement (0.64 ± 0.16 g) ($p < 0.01$). The deceleration rate during the rolling phase of the rollover was not affected by the surface over which it was rolling because there was no relative sliding between the perimeter of the vehicle and the ground.

4. The transition from sliding to rolling typically occurred relatively early in the rollover. On average, vehicles that slid over dirt transitioned from sliding to rolling 19% of the way through the rollover in terms of time, 26% of the way through the rollover in terms of roll angle, and 38% of the way through the rollover in terms of distance. The corresponding numbers for vehicles that slid over pavement were 29%, 35%, and 55% for time, roll angle, and distance, respectively. The peak roll rate is predicted to occur at the time of transition from rolling to sliding.

5. The effective contact point between the perimeter of the vehicle and the ground was always in front of the vehicle's center of gravity when averaged over any particular rollover phase in the rollovers studied. On average, the effective contact point was 1.7 feet in front of the vehicle's center of gravity during the sliding phase of the rollover and 1.3 feet in front of the vehicle's center of gravity during the rolling phase of the rollover.

6. The proposed model can effectively predict rollover dynamics in a "typical" rollover in which the vehicle dynamics follow the general pattern shown in Figure 2. However, in some cases, idiosyncratic impacts can cause unusual rollover dynamics that render the model inapplicable.

The reconstructionist should be alert for evidence of unusual rollover dynamics before attempting to apply this model.

REFERENCES

1. Anderson, J., Gee, R., Germane, G., Henry, K. et al., "Analysis of a Real-World High-Speed Rollover Crash from a Video Record and Physical Evidence," SAE Technical Paper 2008-01-1486, 2008, doi:10.4271/2008-01-1486.

2. Asay, A. and Woolley, R., "Rollover Testing of Sport Utility Vehicles (SUVs) on an Actual Highway," SAE Technical Paper 2010-01-0521, 2010, doi: 10.4271/2010-01-0521.

3. Carter, J., Luepke, P., Henry, K., Germane, G. et al., "Rollover Dynamics: An Exploration of the Fundamentals," *SAE Int. J. Passeng. Cars - Mech. Syst.* 1(1):80-104, 2009, doi:10.4271/2008-01-0172.

4. Chen, H. and Guenther, D., "Modeling of Rollover Sequences," SAE Technical Paper 931976, 1993, doi: 10.4271/931976.

5. Fricke, L.B. Traffic Crash Reconstruction. Northwestern University Center for Public Safety, Evanston, IL. Second Edition, 2010.

6. Funk, J. and Luepke, P., "Trajectory Model of Occupants Ejected in Rollover Crashes," SAE Technical Paper 2007-01-0742, 2007, doi:10.4271/2007-01-0742.

7. Funk, J., Beauchamp, G., Rose, N., Fenton, S. et al., "Occupant Ejection Trajectories in Rollover Crashes: Full-Scale Testing and Real World Cases," *SAE Int. J. Passeng. Cars - Mech. Syst.* 1(1):43-54, 2009, doi: 10.4271/2008-01-0166.

8. Hight, P., Siegel, A., and Nahum, A., "Injury Mechanisms in Rollover Collisions," SAE Technical Paper 720966, 1972, doi: 10.4271/720966.

9. Jones, I. and Wilson, L., "Techniques for the Reconstruction of Rollover Accidents Involving Sport Utility Vehicles, Light Trucks and Minivans," SAE Technical Paper 2000-01-0851, 2000, doi:10.4271/2000-01-0851.

10. Luepke, P., Carhart, M., Croteau, J., Morrison, R. et al., "An Evaluation of Laminated Side Window Glass Performance During Rollover," SAE Technical Paper 2007-01-0367, 2007, doi:10.4271/2007-01-0367.

11. Orlowski, K., Bundorf, R., and Moffatt, E., "Rollover Crash Tests-The Influence of Roof Strength on Injury Mechanics," SAE Technical Paper 851734, 1985, doi: 10.4271/851734.

12. Parenteau, C., Gopal, M., and Viano, D., "Near and Far-Side Adult Front Passenger Kinematics in a Vehicle Rollover," SAE Technical Paper 2001-01-0176, 2001, doi: 10.4271/2001-01-0176.

13. Rose, N., Beauchamp, G., and Fenton, S., "The Influence of Vehicle-to-Ground Impact Conditions on Rollover Dynamics and Severity," SAE Technical Paper 2008-01-0194, 2008, doi:10.4271/2008-01-0194.

14. Rose, N. and Beauchamp, G., "Analysis of a Dolly Rollover with PC-Crash," SAE Technical Paper 2009-01-0822, 2009, doi:10.4271/2009-01-0822.

15. Rose, N. and Beauchamp, G., "Development of a Variable Deceleration Rate Approach to Rollover Crash Reconstruction," *SAE Int. J. Passeng. Cars - Mech. Syst.* 2(1):308-332, 2009, doi:10.4271/2009-01-0093.

16. Searle, J. and Searle, A., "The Trajectories of Pedestrians, Motorcycles, Motorcyclists, etc., Following a Road Accident," SAE Technical Paper 831622, 1983, doi: 10.4271/831622.

17. Stevens, D., Arndt, S., Wayne, L., Arndt, M. et al., "Rollover Crash Test Results: Steer-Induced Rollovers," SAE Technical Paper 2011-01-1114, 2011, doi: 10.4271/2011-01-1114.

18. Thomas, T.M., Cooperrider, N.K., Hammoud, S.A., Woley, P.F., "Real World Rollvoers - A Crash Test Procedure and Vehicle Dynamics Evaluation," Proc. 12th International Technical Conference on Experimental Safety Vehicles, pp. 819-825, 1989.

19. Wilson, L.A., Gilbert, M., Godrick, D.A., "Reconstruction and Analysis of Steering-Induced, On-road, Untripped SUV Rollover Tests (Part 1)," *Collision*, 2(1): 88-113, Summer, 2007.

CONTACT INFORMATION

James R. Funk
Biodynamic Research Corporation
5711 University Heights Blvd., Suite 100
San Antonio, TX 78249
Phone: 210-691-0281
Fax: 210-691-8823
jfunk@brconline.com

ACKNOWLEDGMENTS

We would like to thank Ron Woolley for his assistance with the rollover testing, Michael Bruins for his work in digitizing data from graphs in printed papers, and Don Stevens and his co-authors for sharing their test data with us.

DEFINITIONS/ABBREVIATIONS

a
: Translational acceleration

v
: Translational velocity

d

Translational position

α

Roll acceleration

ω

Roll velocity

θ

Roll angle

m

Vehicle mass

I

Vehicle moment of inertia

k

Vehicle radius of gyration

H

Vehicle height

W

Vehicle width

r

Vehicle radius

g

Gravitational constant (32.2 ft/s^2)

h

Distance forward of vehicle CG where ground force effectively acts on vehicle perimeter

f

Drag factor

t

Time

0

Subscript indicating a value at the time of roll initiation

1

Subscript indicating a value at the time of initial ground contact or during the sliding phase of the rollover

2

Subscript indicating a value at the time when the vehicle stops sliding or during the rolling phase of the rollover

f

Subscript indicating a final value at the end of the rollover

APPENDIX

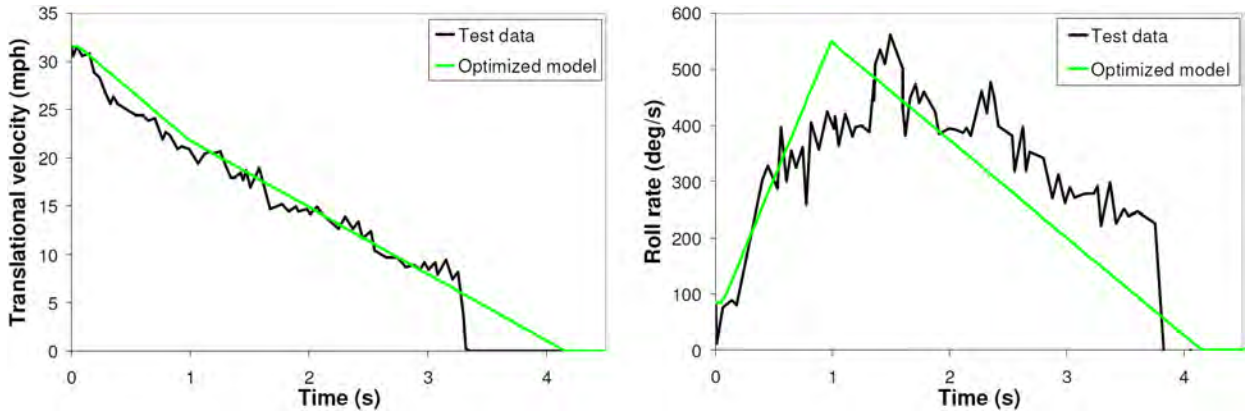

Figure App1. Test data and model fits for test O5.

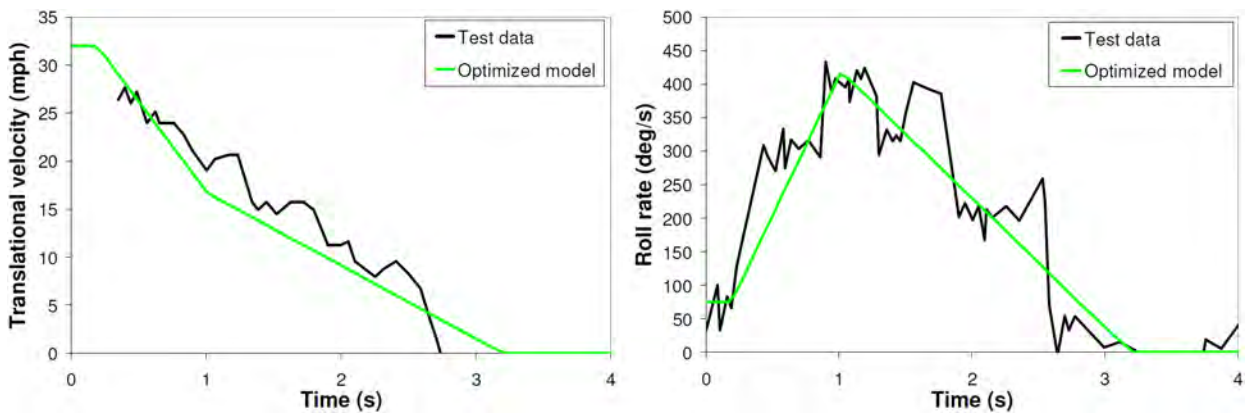

Figure App2. Test data and model fits for test O6.

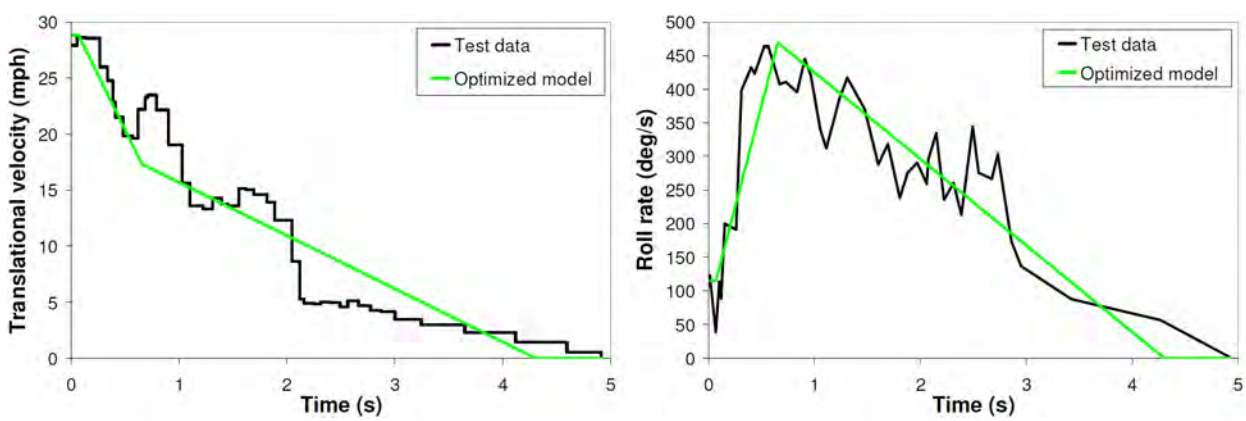

Figure App3. Test data and model fits for test T6.

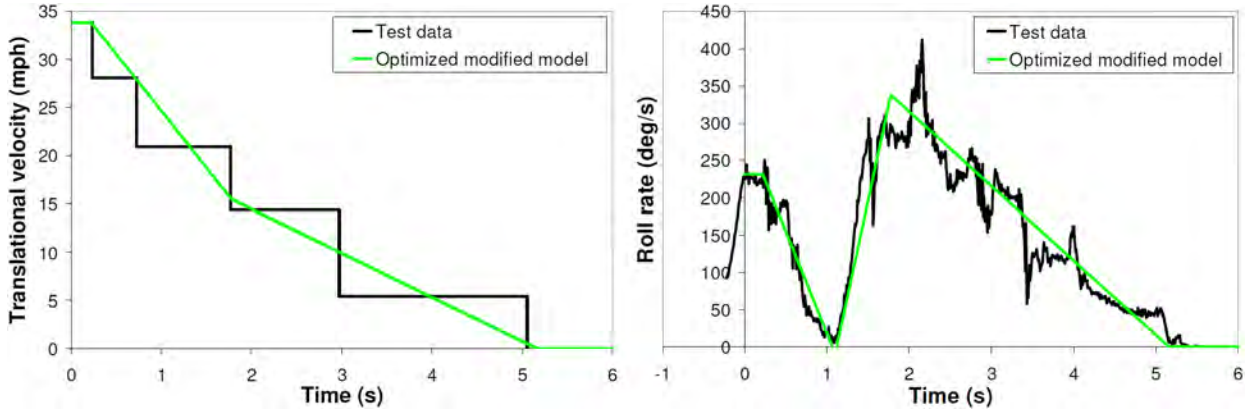

Figure App4. Test data and modified model fits for test S0.

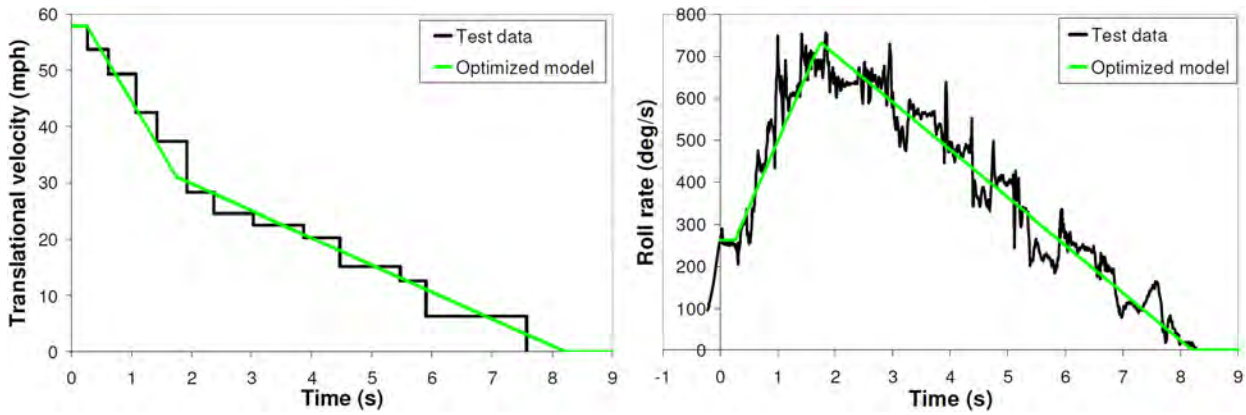

Figure App5. Test data and model fits for test S1.

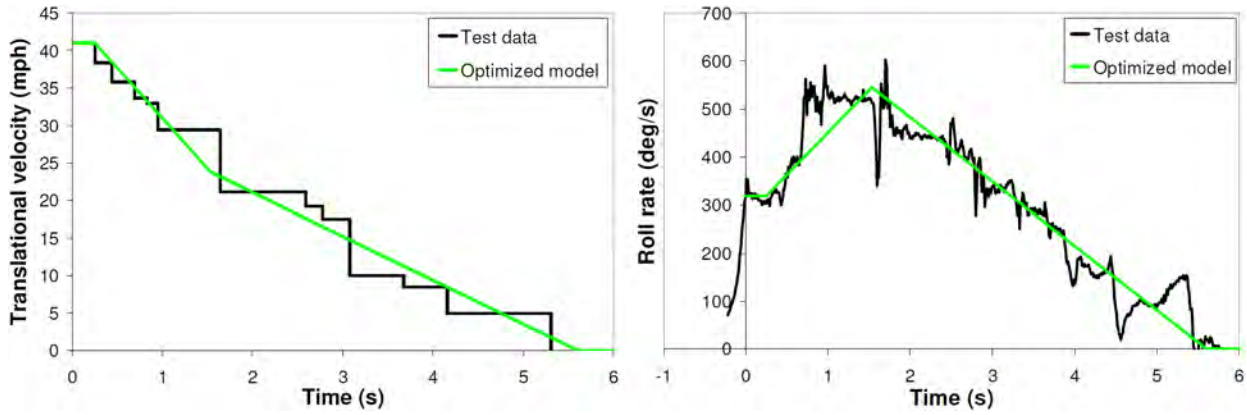

Figure App6. Test data and model fits for test S2.

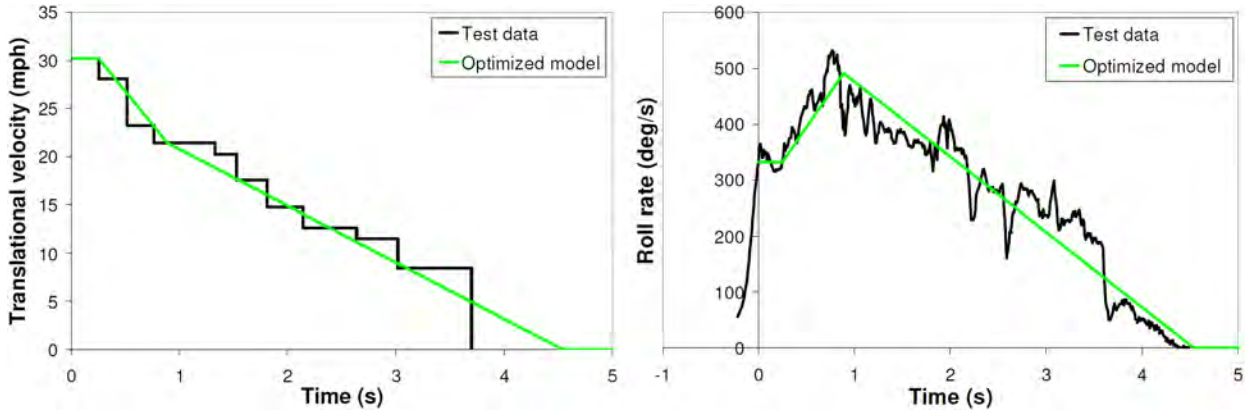

Figure App7. Test data and model fits for test S3.

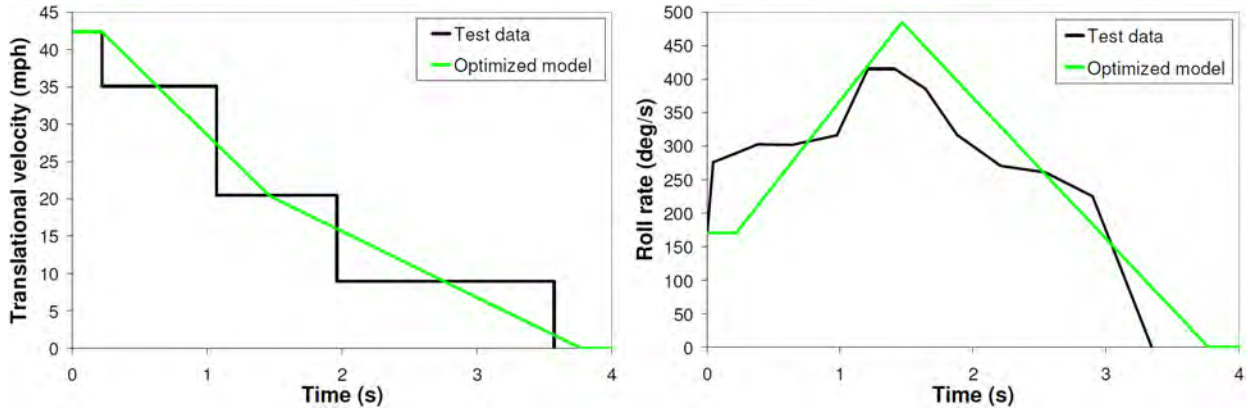

Figure App8. Test data and model fits for test S4.

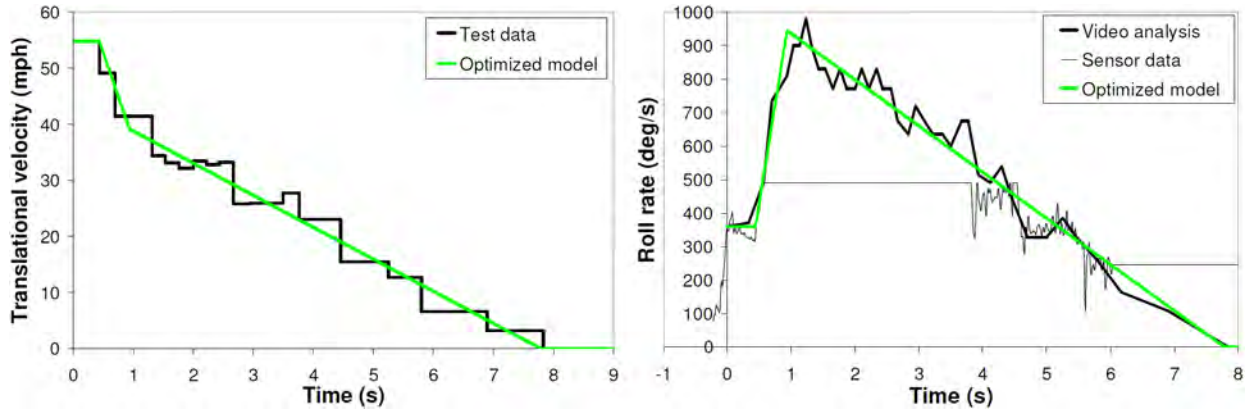

Figure App9. Test data and model fits for test A1. The roll rate sensor clipped during the test, so video analysis was performed to determine roll rate.

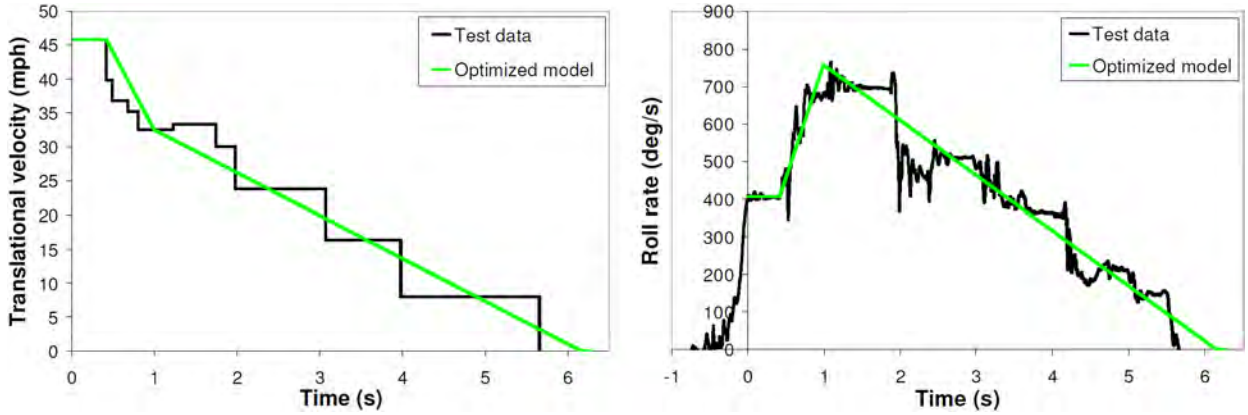

Figure App10. Test data and model fits for test A2.

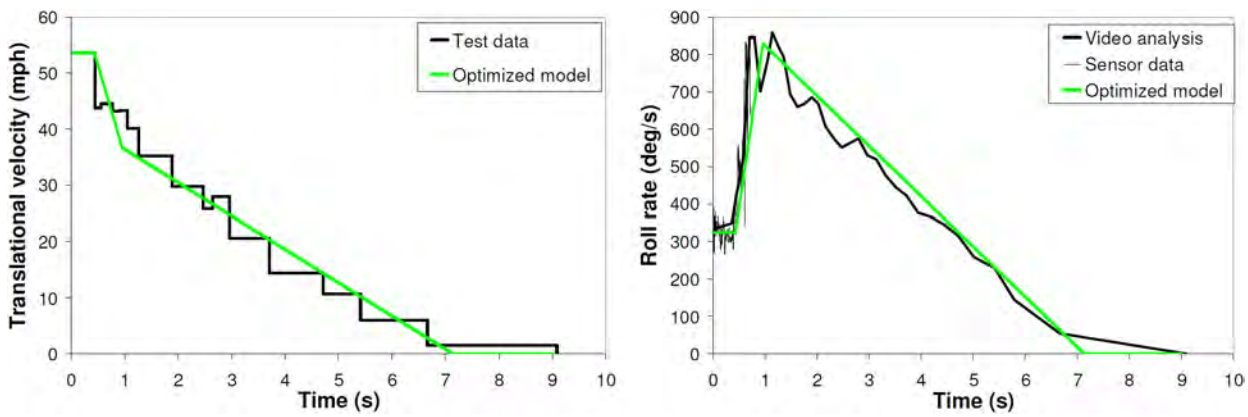

Figure App11. Test data and model fits for test A8. The roll rate sensor failed early in the test, so video analysis was performed to determine roll rate.

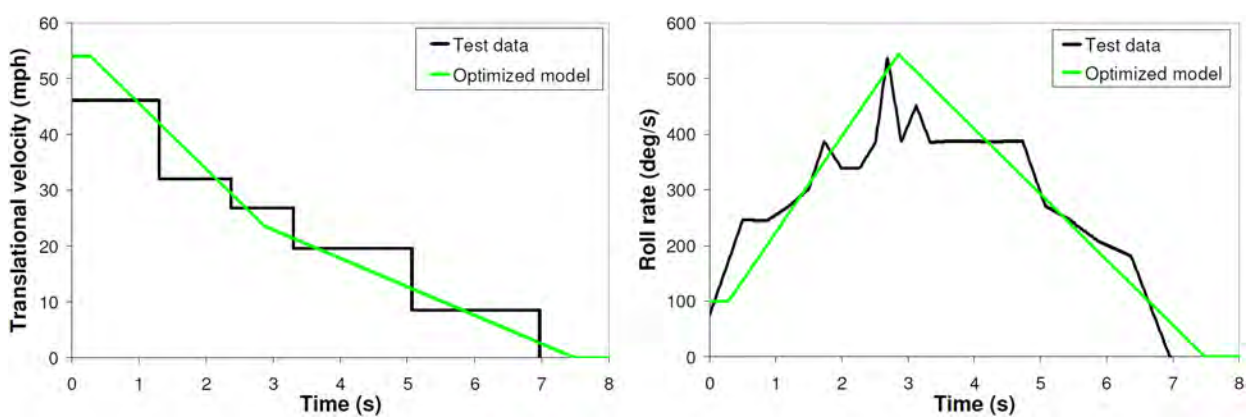

Figure App12. Test data and model fits for test AN.

The Engineering Meetings Board has approved this paper for publication. It has successfully completed SAE's peer review process under the supervision of the session organizer. This process requires a minimum of three (3) reviews by industry experts.

All rights reserved. No part of this publication may be reproduced, stored in a retrieval system, or transmitted, in any form or by any means, electronic, mechanical, photocopying, recording, or otherwise, without the prior written permission of SAE.

ISSN 0148-7191

Positions and opinions advanced in this paper are those of the author(s) and not necessarily those of SAE. The author is solely responsible for the content of the paper.

SAE Customer Service:
Tel: 877-606-7323 (inside USA and Canada)
Tel: 724-776-4970 (outside USA)
Fax: 724-776-0790
Email: CustomerService@sae.org
SAE Web Address: http://www.sae.org
Printed in USA